SURFACE MODIFICATIONS BY SWIFT HEAVY-ION IRRADIATION OF INDIUM PHOSPHIDE

A. S. Khalil [a,b,1], *L. T. Chadderton* [b], *A. Yu. Didyk* [a,2], *M. C. Ridgway* [b], *A. M. Stewart* [b]

[a]Joint Institute for Nuclear Research, Dubna

[b]Research School of Physical Sciences and Engineering, The Australian National University (ANU), Canberra

InP (001) samples were irradiated with 200 MeV Au ions at different fluences. The surface nanotopographical changes due to increasing fluence of swift heavy ions were observed by Atomic Force Microscopy (AFM), where the onset of large increase in surface roughness for fluences sufficient to cause complete surface amorphization was observed. Transmission Electron Microscopy was used to observe formed bulk-ion tracks in InP and high resolution TEM (HRTEM) revealed that single-ion tracks might not be amorphous in nature. Surface-ion tracks were observed by AFM in the form of ill-defined pits (hollows) of $\sim$ 12 nm in diameter (width). In addition, Rutherford backscattering was utilized to follow the formation of disorder to amorphization in the irradiated material. The interpretation of large increase in surface roughness with the onset of amorphization can be attributed to the plastic phenomena induced by the change of states from crystalline to amorphous by ion irradiation.

Образцы InP (001) были облучены ионами Au с энергией 200 МэВ при различных флюенсах. Структура поверхностной топографии облученных образцов в зависимости от флюенса облучения быстрыми тяжелыми ионами была изучена методом атомно-силовой микроскопии (АСМ). Обнаружено, что при полной аморфизации поверхности на ней происходят значительные изменения. Метод просвечивающей микроскопии был использован для изучения объемной структуры ионных треков, и с помощью микроскопии высокого разрешения (HRTEM) обнаружено, что треки ионов не являются аморфными. Поверхность ионных треков исследована АСМ-методом, и показано, что их форма представляет собой ямки диаметром примерно 12 нм. Обнаруженные большие неоднородности на поверхности облученных образцов при больших флюенсах облучения с практически полной ее аморфизацией могут быть объяснены значительными механическими упругими напряжениями, которые возникают при перестройке решетки от кристаллического к аморфному состоянию с возрастанием средней постоянной решетки.

PACS: 34.50.-s; 61.80.Lj; 61.80.-x

INTRODUCTION

Spectacular topography and surface changes occur when irradiating semiconductors with swift heavy ions (SHI) [1–6]. It is known that amorphous materials when bombarded with SHI exhibit dramatic surface and shape changes or macroscopic plastic deformations [7, 8].

---

[1]E-mail: Ali.Khalil@anu.edu.au
[2]E-mail: didyk@jinr.ru

This effect was found to occur particularly in amorphous or amorphizable solids, but was not observed in materials which remain crystalline during SHI irradiation. In general, covalent materials which exhibit irreversible density changes due to amorphization such as elemental semiconductors Si were found to prominently exhibit mass transport and plastic deformation under SHI irradiation after reaching ion fluences sufficient to cause complete amorphization [9]. In addition, the elastic constants of irradiated materials are expected to change drastically only when the material becomes amorphous in the case of many semiconductors. For example, it was shown that the shear modulus of irradiated Si only showed a drastic reduction when it became completely amorphous and very little elastic softening was observed even for heavily damaged Si [10]. Thus, once an amorphous layer is formed, radiation-induced plastic flow and deformation of material out of the plane of the irradiated surface occur, as this might relieve the stress created by the changes in density and the elasticity of the amorphous material. In the case of SHI irradiation, this can also be attributed to the thermal spike induced by intense electronic excitation and the consequent relaxation of the thermo-elastic shear stress in the hot cylindrical core of the track, where stresses of the order $\sim 10^8$ N/m^2 can develop transiently in the ion wake, leading to plastic phenomena [11, 12]. The transient tracks in amorphous materials can be treated as ellipsoidal elastic inclusions in elastically isotropic media and the corresponding strain increment will be *quenched-in* upon rapid cooling of the transient track, so as to produce the overall plastic deformation [13, 14]. Similar density changes as that of Si occur in the case of the compound semiconductor InP, where this material compacts when amorphous. In a relaxed state, amorphous InP is $\sim 0.17\%$ more dense than crystalline InP and it even increases by $\sim 7\%$ in a molten state [15, 16]. This may be the case inside the track core during the very short transient time ($\sim$ picoseconds) of track registration which leads to large transient stresses during the lifetime of the core, whilst still in a liquid-like state. For the case of irradiated amorphous materials, the transient tracks cannot recrystallize by homoepitaxial recrystallization and this may lead to transient stress build-up giving rise to prominent macroscopic plastic changes observed after reaching complete amorphization [13].

Once more it should be stressed that SHI-induced mass transport and flow arising from plastic behaviour in semiconductors are a phenomenon observed only when the semiconductors become amorphous. Thus, formation of an amorphous state becomes a crucial parameter in elastic and mass transport phenomena, since an amorphous state has different elastic and transport constants compared to a crystalline or even heavily damaged surface, which presents a different scenario for a transient track in the wake of SHI. As recently shown by Hedler et al. [18], Si under 350 MeV Au$^+$ ion irradiation flows plastically when it becomes completely amorphous as ion fluences reach $\sim 1.7 \cdot 10^{15}$ cm^{-2}. In another interesting observation, 30 MeV Cu$^+$ ions induced anisotropic deformation even in amorphous Si micron-sized structures, whilst the crystalline counterparts showed no change [18]. Not only semiconductor microstructures, but even if the irradiated semiconductor is in the form of a restrained thin wafer, the stress generated will be microscopically manifested as a curvature of the wafer's surface only after reaching complete amorphization as observed for InP [19]. Observations of Si wafers irradiated with 100 MeV Au$^+$ ions showed also a large increase of surface roughness when ion fluences reach levels to cause complete amorphization [1]. A similar behaviour was observed for InP irradiated with 24 MeV Si ions, where deformation under the energetic ions only begins when InP becomes amorphous and where oblique conditions of irradiation can create structures such as «*ditch*» and «*dike*» after amorphization, due to

macroscopic surface collective displacements [17]. In this study, we report the observation of drastic surface modification of (001) InP after reaching complete amorphization by 200 MeV Au ion irradiation.

EXPERIMENTAL

InP samples were prepared for irradiation from a 500 μm thick, semi-insulating, polished, (001) oriented wafer; each sample being scribed and cut into pieces of $\sim 10 \times 10$ mm for ion irradiation. In addition to bulk samples, samples in the form of electron-transparent thin foils were simultaneously irradiated for subsequent transmission electron microscopy investigation. The SHI irradiation was performed at room temperature using the 14 UD Pelletron accelerator at the Nuclear Physics Department of the Australian National University. The bulk samples were fixed to a copper plate using conductive Ag paste, while the thin foil samples were placed in specially designed aluminium holders. The pressure inside the irradiation chamber was $\sim 10^{-7}$ Torr maintained by a turbo-molecular pump. The irradiation fluences ranged from $5 \cdot 10^{10}$ to $1 \cdot 10^{14}$ cm^{-2}. The ion flux (fluence-rate) was maintained at $\sim 6.2 \cdot 10^9$ cm$^{-2} \cdot$ s^{-1} to avoid any adverse heating effects. The dosimetry during irradiation was monitored by charge integration. Exact total dosimetry was determined from TEM observations of simultaneously irradiated MoO_3 crystallites for the lower-ion fluences. The irradiated bulk samples were subsequently analyzed by Rutherford backscattering with 2 MeV He$^+$ ions to assess the progression of damage until complete amorphization. Philips 300 CM and JEM-2010 F transmission electron microscopes were used for TEM investigations. The evolution of the InP (001) surface as a function of the 200 MeV Au$^+$ ion fluence was studied by atomic force microscopy (AFM). The chosen variable was the root mean square roughness (RMS), which is the standard deviation of height values Z within the probed scanned area. This quantity is defined as

$$\text{RMS} = \sqrt{\sum_{i=1}^{N} \frac{(Z_i - Z_{\text{ave}})^2}{N}}, \tag{1}$$

where Z_{ave} is the average height within the scanned area; Z_i is the measured height at a given point i and N is the number of points within the scanned area.

Different areas of 1×1 μm and less were scanned in the irradiated and unirradiated regions of each sample under ambient conditions in contact mode. The AFM images in the course of this work were acquired at ambient laboratory conditions using Nanoscope III AFM with Si commercially cantilever tips with a nominal radius of curvature for the apex ~ 10 nm. The scanned AFM images had 512×512 point resolution. The RMS determination was performed using the attached commercial Nanoscope III (R) software. The RMS values were obtained after first-order image «flattening» for each acquired AFM image. The flattening routine basically removes noise in the form of observed *bow* introduced into the AFM image due to the tip-scanner configuration by calculating least-squares fitted second-order polynomial for each scan line, then subtracting it from the scan line, thus leveling the background of the image without any loss of information.

RESULTS AND DISCUSSION

Figure 1 illustrates two-dimensional AFM images of scanned 500×500 nm areas for unirradiated and 200 MeV Au^+ irradiated InP for different ion fluences. The AFM image for unirradiated InP showed a relatively smooth (001) surface profile on that scale

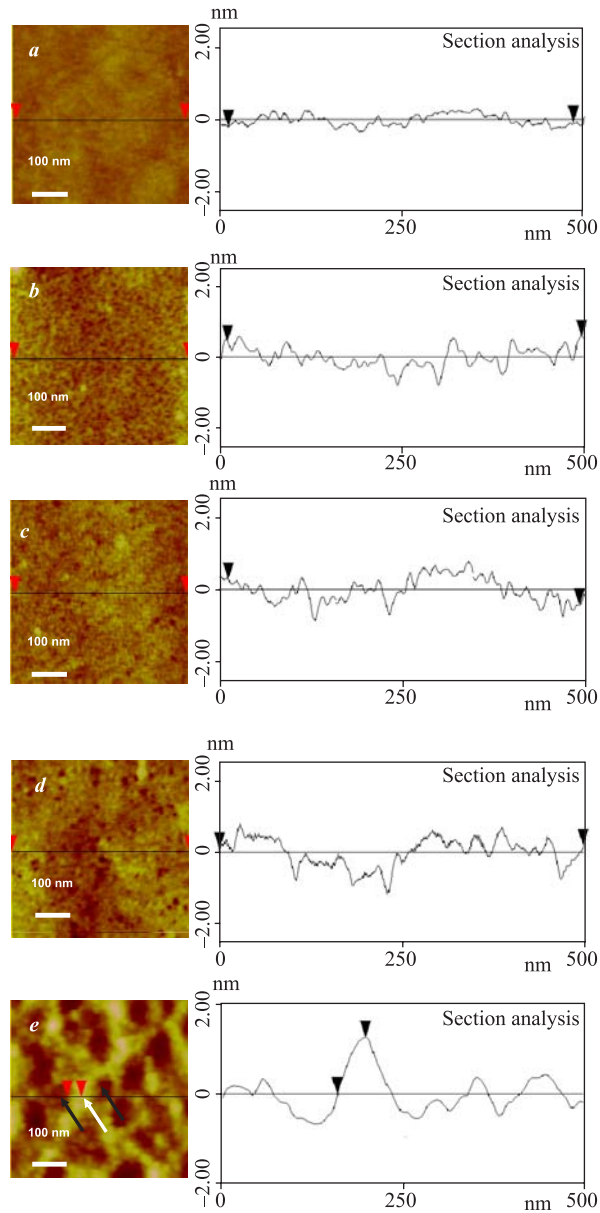Fig. 1. The AFM images of 500×500 nm scanned areas and sectional analyses across the surface of unirradiated InP (*a*) for $5 \cdot 10^{10}$ cm^{-2} (*b*), $5 \cdot 10^{12}$ cm^{-2} (*c*), $1 \cdot 10^{13}$ cm^{-2} (*d*) and $1 \cdot 10^{14}$ cm^{-2} (*e*) irradiated InP

(2 nm/division) as indicated by the sectional analysis across the surface. For the lowest ion fluence ($5 \cdot 10^{10}$ cm^{-2}) the surface profile is also relatively smooth with very small-observed change as evidenced in the accompanied sectional analysis. Also, no large change in roughness occurs, when the ion fluence reaches $5 \cdot 10^{12}$ cm^{-2}, except the observed finer *crinkling* across the surface profile as evident in the sectional analysis in Fig. 1, *c*. This implies that the roughening on that scale is due to the increased ion impacts on the surface with increasing ion fluences as expected. For the $1 \cdot 10^{13}$ cm^{-2} irradiated surface almost no change is evident (Fig. 1, *d*). Conversely, for the highest fluence irradiated InP surface ($1 \cdot 10^{14}$ cm^{-2}), which is now completely amorphous, the surface becomes very rough compared to the unirradiated and low-fluence irradiated surfaces. The AFM observations reveal hillock-like features or protrusions (as the one pointed by the white arrow) accompanied by trough-like features (pointed by black arrows).

This nanoscale topographical change for the amorphous surface is more clearly visualized in Fig. 2, where three-dimensional projections of AFM images of both unirradiated and the
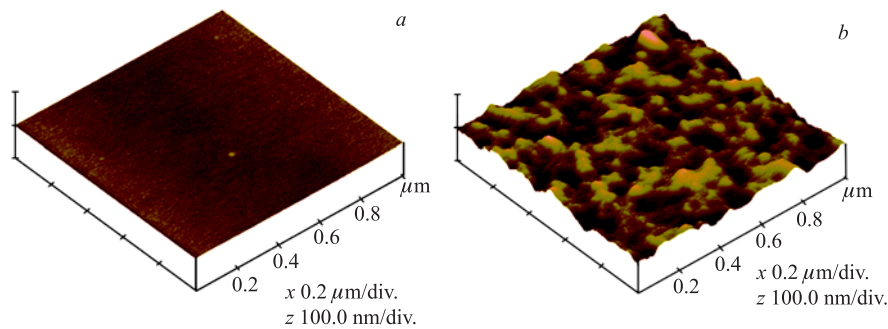

Fig. 2. Three-dimensional projected AFM images of 1×1 μm scanned areas of unirradiated InP (*a*) and $1 \cdot 10^{14}$ cm^{-2} irradiated InP surface (*b*). Vertical scale = 100 nm/div.
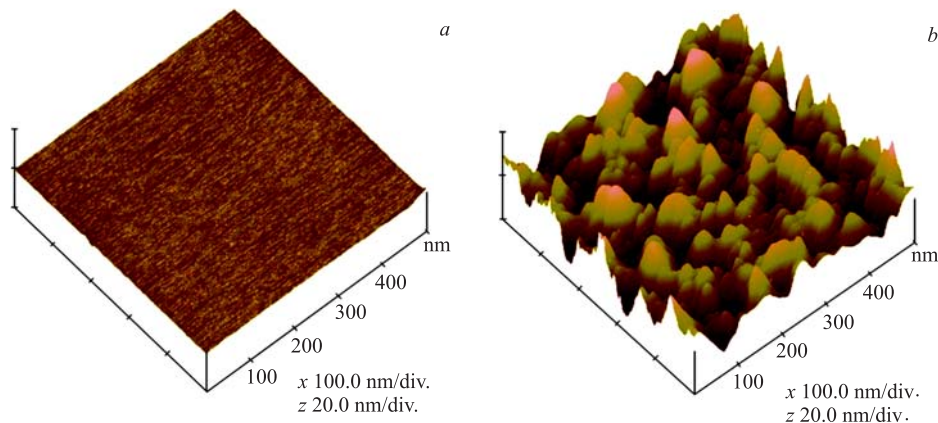

Fig. 3. Three-dimensional projected AFM images of 500×500 nm scanned areas of an area unexposed to the ion beam for the $1 \cdot 10^{14}$ cm^{-2} irradiated InP sample (i.e., still crystalline) (*a*) and irradiated area of the same sample (amorphous) (*b*). Vertical scale = 20 nm/div.

highest-ion fluence irradiated InP are shown together. The observed nanotopography change is obvious and might imply nanoscopic material transfers evident from the rugged amorphous InP surface comprising the protruded hillocks accompanied by troughs.

In Fig. 3 we show three-dimensional projected AFM images of two areas of the same irradiated InP sample $(1 \cdot 10^{14}$ cm$^{-2})$, the unirradiated area of the sample (i.e., an area unexposed to the 200 MeV Au$^+$ beam, and therefore remaining crystalline) which remains smooth, whereas the irradiated area of the same sample is quite rough.

On the other hand, for the low-fluence ion-irradiated surfaces, we have not observed well-defined surface-ion tracks (a surface-ion track is the *imprint* of single SHI impact onto the surface which can be observed, for example, as a prominent hillock, crater as observed for two other materials — muscovite mica and molybdenum disulphide irradiated simultaneously with the InP samples). Instead we have observed pit-like features for the lower fluences irradiated InP surfaces. These pits are thought to be surface-ion tracks in InP as a result of 200 MeV Au$^+$ ion impacts. This is shown in the AFM scan of an area of 100×100 nm in Fig. 4. Sectional analyses across such pits show that the average pit width is to be $= (12.3 \pm 2.3)$ nm. These widths are in good agreement with our observation of the bulk 200 MeV Au$^+$ ion tracks in InP as revealed by TEM in Fig. 5, where Fig. 5, a shows a field of ion tracks and Fig. 5, b is high magnification bright field TEM, which depicts two such tracks, the track diameter
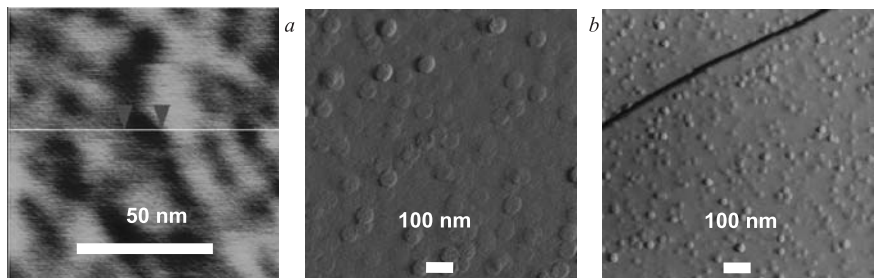

Fig. 4. The AFM image of 100×100 nm scanned area of InP irradiated with fluence of $5 \cdot 10^{10}$ cm^{-2} showing a pit-like feature identified with surface-ion tracks due to single 200 MeV Au$^+$ ion impact, the width of the pit ~ 12.5 nm. In a initial surface is shown. In b and c AFM images of 1×1 μm scanned area of both muscovite mica and molybdenum disulphide respectively irradiated to the same ion fluence depicting the observed prominent surface-ion tracks are shown
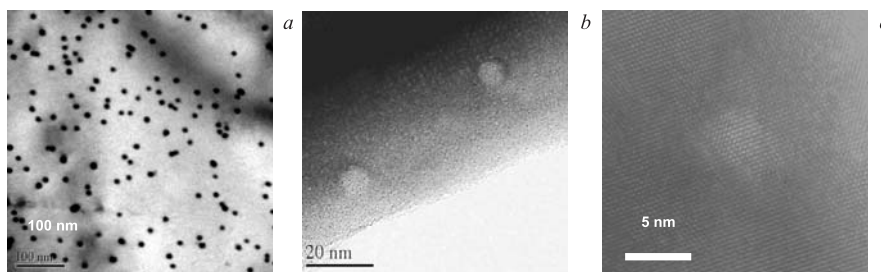

Fig. 5. Bulk ion tracks observed by TEM in InP: a) a field of ion tracks; b) a high magnification TEM of two tracks; c) HRTEM of a single ion track

is around ~ 8 nm. In Fig. 5, *c* we show a high resolution TEM of such a track, where it appears that lattice fringes appear over the track core (~ 5 nm in width) implying that the track core is not amorphous in nature and the crystallinity of material is preserved upon a single 200 MeV Au^+ ion impact. In the AFM scanned area of 100×100 nm we expect to find on the average ~ 5 pits (since at this ion fluence of $5 \cdot 10^{10}$ cm^{-2} we expect on the average ~ 5 tracks per each 100×100 nm area). This was confirmed by TEM observation of dosimetric MoO_3 crystallites irradiated simultaneously with InP, where a one-to-one correspondence was found between the ion fluence and ion track densities for the lower fluence irradiated samples.

The difficulty of observing the anticipated *well-defined* surface-ion tracks (identified with these nanoscale pits) by AFM in InP may be due to AFM tip convolution effects. This combination of tip-surface effects attributed to the geometry, shape and fineness of the tip apex relative to the imaged features, which can affect the final resolution (both lateral and depth) and the final observed appearance in AFM imaging of such small nanoscale features like surface-ion tracks in InP. The widths of surface-ion tracks in InP might not be different than the tracks inside the material (bulk tracks as revealed by TEM); in this case, they are comparable in size to the AFM scanning tips (the Si tip apex radius of curvature ~ 10 nm), for example, muscovite mica and molybdenum disulphide showed prominent hillocks and craters respectively identified as surface 200 MeV Au^+ ion tracks of average widths of ~ 60 nm for the former and ~ 70 nm for the later material, which are much larger in size than the apex diameter of the scanning AFM Si tip. In addition to that, another factor can simply explain the lack of observing well-defined and prominent surface-ion tracks in InP, mainly that there are no strong 200 MeV Au^+ ion-surface effects when an ion impacts on the crystalline InP surface (e.g., Coulomb explosion or large sputtering yields, which can result, for example, in an observation of hillock or crater around an ion impact, respectively). Previous AFM observations on 100 MeV Au^+ ion irradiated (111) InP surface to a fluence of $1 \cdot 10^{12}$ cm^{-2} due to Singh et al. [4] revealed similar features to our observed pit-type features but with larger *diameter* of ~ 24 nm with an areal density corresponding to the ion fluence. They were identified as surface-ion tracks, while no such features were observed for 180 MeV Ag^+ irradiation of (111) InP.

As mentioned above, the important observation revealed by our AFM is the development of large increase in surface roughness when the irradiated surface becomes completely amorphous. Figure 6 shows a typical sequence of projected AFM scans for InP (001) irradiated surfaces at different ion fluences, which clearly demonstrate the observed surface evolution with increased ion fluences. The large change only occurs for higher fluences $\geqslant 5 \cdot 10^{13}$ cm^{-2}, where a drastic increase takes place revealed as the multiple protrusions of hillock on nanoscale. A plot of RMS roughness as a function of fluence is shown in Fig. 7. The RMS roughness increases dramatically for higher fluences at $5 \cdot 10^{13}$ cm^{-2} with a slight decrease for the $1 \cdot 10^{14}$ cm^{-2} ion fluence. This decrease may be attributed to slight smoothing of hillocks because of local variation in the angle of ion incidence due to the already developed nanoroughness during ion irradiation. This is similar to the observation in SHI irradiated Si, where the height of the hillock-like features decreases for the highest fluence at $1 \cdot 10^{14}$ cm^{-2} [15]. Another similar observation for (001) InP irradiated by 150 MeV Fe ions was a decrease in roughness for the same fluence of $1 \cdot 10^{14}$ cm^{-2} [6]. Even for low-energy irradiations, quite similar observations were reported for surface topography of GaAs (110) after high fluence low-energy Si^+ ion irradiation, where the height of the observed hillock-like protrusions increases up to certain fluence saturation level [20]. The
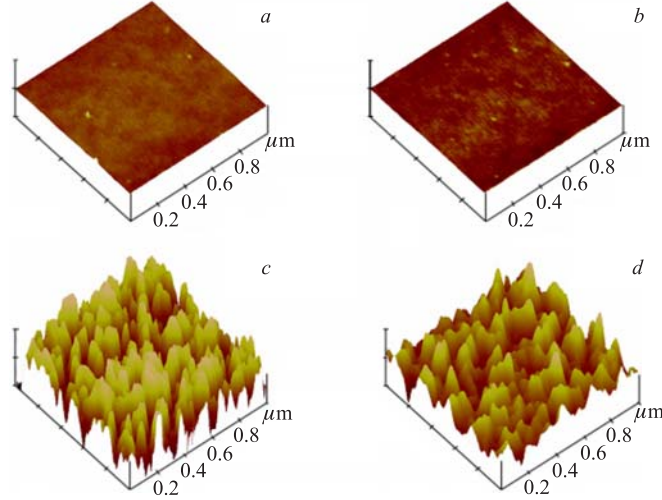
Fig. 6. Three-dimensional projected AFM images of 1×1 μm scanned areas of unirradiated surface (*a*), $1 \cdot 10^{11}$ (*b*), $5 \cdot 10^{13}$ (*c*) and $1 \cdot 10^{14}$ cm^{-2} (*d*) irradiated (001) InP surfaces. The surfaces for lower fluence irradiations are smooth on that scale (the height scale for all scans is 20 nm/division). The significant increase in surface roughness only occurs for higher fluences when the surface becomes completely amorphous. The observed surface modification in the form of hillock-like features is evident for the two highest ion fluences

amount of relative disorder $\Delta\chi_{\mathrm{min}}$ extracted from the RBS/C yield (Y) is also plotted in the same plot for RMS in Fig. 7 and defined as:

$$\Delta\chi_{\mathrm{min}} = \frac{Y_{\mathrm{irrad}} - Y_{\mathrm{unirrad}}}{Y_{\mathrm{random}} - Y_{\mathrm{unirrad}}}. \tag{2}$$

The value of $\Delta\chi_{\mathrm{min}}$ expresses the relative amount of disorder in the crystal and approaches unity for complete amorphization at a fluence of $\sim 5 \cdot 10^{13}$ cm^{-2} as shown in Fig. 7 (the solid line), which indicates the progression towards complete amorphization. In addition, the inset in Fig. 7 shows the TEM observation for the $5 \cdot 10^{13}$ cm^{-2} irradiated InP (which is completely amorphous as revealed by electron diffraction). A similar trend of RMS roughness increase in 100 MeV Au$^+$ ion irradiated InP (111) surfaces at room temperature was observed by Singh et al. [5]. They attributed this to thermal spike induced effects and subsequent relaxation. In their observations for irradiation at lower temperature (96 K) the increase in roughness was less pronounced than at room temperature, due to the suppression of track formation at 96 K because of the high thermal conductivity of InP at that temperature. In the work of Dubey et al. [6] for 100 MeV Fe ion irradiated (001) InP similar observation of drastic surface roughness increase was made after ion fluences reached sufficient fluences to cause observation of peaks on the surface and high resolution X-ray diffraction (HRXRD) spectra. As indicated by our TEM observations, each impinging 200 MeV Au$^+$ ion creates a single track with *core width* of ~ 5 nm. Our HRTEM observations (Fig. 5) showed that the ion tracks might not be amorphous in nature, so that, in order to render an area of InP, amorphous, multiple ion impacts and track overlap may be required, thus the process of amorphization proceeds with
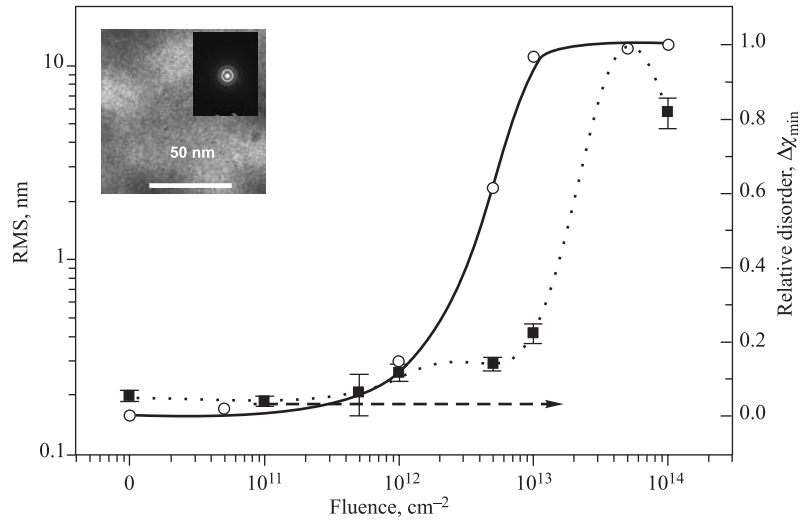
Fig. 7. The RMS roughness as a function of 200 MeV Au$^+$ ion fluence in InP (dotted line). The relative disorder induced by irradiation (solid line) is also plotted. The inset is TEM micrograph of InP irradiated to fluence of $5 \cdot 10^{13}$ cm^{-2}, where the selected area diffraction pattern shows the diffused rings synonymous with amorphous material

the increasing ion fluence as statistically expected [21]. Therefore, the amorphous fraction of material must be expected to increase with increasing fluence. The multiple ion impact on process required for amorphization in SHI irradiated InP was also reported by O. Herre et al. [22] for 250 MeV Xe$^+$ irradiated InP, where the authors used a simple Gibbons overlap model [23] to fit their $\Delta\chi_{\min}$ data and inferred that at least 3 to 4 ions must impact on the same area to produce an amorphous material. This in general accords with our observations. At $\leqslant 5 \cdot 10^{13}$ cm^{-2} an InP surface will be completely amorphized. The observed drastic roughening of the surface after complete amorphization can generally be attributed to the ion-induced plastic deformation phenomenon, which invokes the difference in the final elastic and transport constants of the completely amorphized surface from these for crystalline or heavily disordered material. After complete amorphization subsequent impinging ions now impact on a surface which is in a completely different state than the crystalline surface, whose difference in the final elastic and transport properties may in turn well affect the structural relaxation through stress build-up due to the transient tracks, which now form in the amorphous material [24]. For example, it is well known that for the case of metallic glasses (where the first observation of ion-induced plastic deformation was made in the early 1980s) there is a small $\sim 2\%$ difference in densities between the amorphous phases relative to their crystalline counterparts. However, the differences in both the bulk and shear moduli are larger $\sim 7\%$ and ~ 30 to 50%, respectively [25]. This might be the case for InP. The elastic softening (reduction in elastic constants relative to that of crystalline phase) in amorphous tetrahedral semiconductors (including both elemental and III–V semiconductors such as InP) can be comparable in magnitude and even higher as they have similar origins to that of metallic glasses, i.e., the internal atomic displacements and the existence of a free volume in amorphous phases or internal relaxation process in the disordered atomic

network [26]. Theoretical calculations predicted elastic softening for both elemental and compound semiconductors upon amorphization, which can be varied over a wide range (of ~ 5 to 50%) depending on the network model and the atomic interaction potential [27, 28].

Therefore, softening of elastic moduli is a generic property in both elemental and compound semiconductors leading to associated plastic phenomena [29]. However, it is not yet clear either what exact factors define the magnitudes of the elastic softening effects for amorphous states, or what features of atomic interactions are important in this respect [30]. However, substantial elastic softening of $\sim 20-50\%$ of both the bulk (Young's) and shear elastic moduli has been experimentally observed for amorphous phases of different elemental semiconductors such as Si and Ge [10, 31] and compound semiconductors such as GaAs [32] GaSb [30] and GaP [33]. This reduction in elastic constants is expected to greatly affect the elastic behaviour of irradiated semiconductors after complete amorphization, which can be manifested in the large surface roughening as in our AFM observations and associated plastic phenomena. To our best knowledge there exist no reliable, comprehensive or experimental data for the elastic moduli or constants in amorphous InP. This makes any quantification of the ion-induced plastic deformation in that material a difficult and challenging problem.

CONCLUSIONS

Surface-ion tracks in InP were observed by AFM as pit-like features for low SHI fluences. The difficulty of observing well-defined surface tracks in InP may be due to AFM tip convolution effects as surface-ion tracks in InP are small in widths or that individual ion impacts on the surface cannot be well-discernible such as in the case of well-defined craters as observed, for example, in mica and MoS_2. Our observation of drastic nanotopographical change for higher irradiating SHI fluences, where the change in root mean square roughness (RMS) showed a large increase only after the surface becomes completely amorphous, suggests the crucial role of SHI irradiation-induced states in InP with increasing ion fluences and that subsequent elastic softening of the amorphous phase relative to that of crystalline phase in that material are important and may give rise to the associated ion-induced plastic phenomena manifesting itself as large increase in surface roughness.

REFERENCES

1. *Srivastava P. C., Ganesan V., Sinha O. P.* // Nucl. Instr. Meth. B. 2002. V. 187, No. 2. P. 20–230.
2. *Srivastava P. C., Ganesan V., Sinha O. P.* // Rad. Meas. 2003. V. 36, Nos. 1–6. P. 671–674.
3. *Srivastava P. C., Ganesan V., Sinha O. P.* // Nucl. Instr. Meth. B. 2004. V. 222, Nos. 3–4. P. 491–496.
4. *Singh J. P. et al.* // Nucl. Instr. Meth. B. 2001. V. 179. P. 37–41.
5. *Singh J. P. et al.* // J. Appl. Phys. 2001. V. 90, No. 12. P. 5968–5972.
6. *Dubey R. L. et al.* // Nucl. Instr. Meth. B. 2007. V. 257, Nos. 1–2. P. 287–292.
7. *Klaumunzer S., Shumacher G.* // Phys. Rev. Lett. 1983. V. 51, No. 21. P. 1987–1990.
8. *Hou M., Klaumunzer S., Shumacher G.* // Phys. Rev. B. 1989. V. 41, No. 2. P. 1144–1157.
9. *Demkowicz M. J., Argon A. S.* // Phys. Rev. Lett. 2004. V. 93, No. 2 (Art. No. 025505).
10. *Bhadra R.* // Phys. Rev. B. 1998. V. 38, No. 17. P. 12656–12659.

11. *Volkert C. A. //* J. Appl. Phys. 1991. V. 70, No. 7. P. 3521–3527.

12. *Volkert C. A., Polman A. //* Materials Research Symp. Proc. 1992. V. 235. P. 3–14.

13. *Trinkaus H., Ryazanov A. I. //* Phys. Rev. B. 1995. V. 74, No. 25. P. 5072–5075.

14. *Chicoine M. et al. //* Phys. Rev. B. 1997. V. 56, No. 3. P. 1551–1560.

15. *Cliche L., Roorda S., Masut R. A. //* Nucl. Instr. Meth. B. 1996. V. 96, Nos. 1–2. P. 319–322.

16. *Cliche L., Roorda S., Masut R. A. //* Appl. Phys. Lett. 1994. V. 65, No. 14. P. 1754–1756.

17. *Khalil A. S.* JINR Preprint E14-2007-173. Dubna, 2007.

18. *Hedler A., Klaumunzer S. L., Wesch W. //* Nature Materials. 2004. V. 3. P. 804–809.

19. *van Dillen T. et al. //* Appl. Phys. Lett. 2004. V. 84, No. 18. P. 3591–3593.

20. *Schmuki P. et al. //* Appl. Phys. Lett. 1997. V. 70, No. 10. P. 1305–1307.

21. *Riedel C., Spohr R. //* Rad. Effects. 1979. V. 42. P. 69–75.

22. *Herre O. et al. //* Phys. Rev. B. 1998. V. 58, No. 8. P. 4832–4837.

23. *Gibbons J. F. //* Proc. of the Inst. of Electrical and Electronics Engineers. 1972. V. 60, No. 9. P. 1062–1096.

24. *Colin J., Lesueur D., Grilhe J. //* Philos. Mag. A. 2001. V. 81, No. 4. P. 857–866.

25. Glassy Metals II. Topics in Applied Physics / Eds.: Beck H., Guntherdot H. J. Berlin: Springer-Verlag, 1983. V. 53.

26. *Brazhkin V. V. et al. //* J. Non-Crystalline Solids. 1997. V. 212. P. 49–54.

27. *Feldman J. L., Broughton J. Q., Wooten F. //* Phys. Rev. B. 1991. V. 43, No. 3. P. 2152–2158.

28. *Kluge M. D., Ray J. R. //* Phys. Rev. B. 1988. V. 37, No. 8. P. 4132–4136.

29. *Mathioudakis C., Kelires P. C. //* J. Non-Crystalline Solids. 2000. V. 266/269. P. 161–165.

30. *Brazhkin V. V. //* Phys. Rev. B. 1997. V. 56, No. 3. P. 990–993.

31. *Testardi L. R., Hauser J. J. //* Solid State Commun. 1977. V. 21, No. 11. P. 1039–1041.

32. *Sharma R. P. et al. //* J. Appl. Phys. 1989. V. 66, No. 1. P. 152–155.

33. *Zuk J., Kiefte H., Clouter M. //* J. Appl. Phys. 1993. V. 73, No. 10. P. 4951–4954.